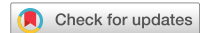


scientific data



OPEN

DATA DESCRIPTOR

Mapping global land conversion pressure to support conservation planning

James Oakleaf¹✉, Christina Kennedy², Nicholas H. Wolff³, Drew E. Terasaki Hart^{4,5}, Peter Ellis⁴, David M. Theobald⁶, Brandie Fariss¹, Karl Burkart⁷ & Joseph Kiesecker¹

Proactively identifying where land conversion might occur is critical to targeted and effective conservation planning. Previous efforts to map future habitat loss have largely focused on forested systems and have been limited in their consideration of drivers of loss. We developed a 1-km resolution, global map of land conversion pressure from multiple drivers, referred to as the conversion pressure index (CPI). The CPI combines past rates of anthropogenic change, as measured by temporal human modification maps, with suitability maps for potential future expansion by large-scale development. The CPI thus offers a new way to measure a cumulative gradient of anthropogenic pressure as opposed to categorical land cover change. We find that nearly 23% of land across 200 countries have relatively high conversion pressure, potentially impacting over 460 million ha of intact natural lands. We illustrate how this information can be used to identify areas for proactive conservation to avoid future loss and ensure that national commitments under the Kunming-Montreal Global Biodiversity and Paris Agreement Climate Frameworks are upheld.

Background & Summary

Anthropogenically-induced habitat change has increased dramatically over the past 25 years¹, causing widespread losses to global biodiversity and nature's benefits to people^{2,3}. Given limited capital and resources, targeted and proactive conservation on at-risk lands will be required to effectively halt further habitat loss and degradation. Foundational to this is an understanding of where future conversion pressure may intersect with existing conservation assets (e.g., natural habitats, species richness, carbon reserves) so that appropriate actions (e.g., protection, improved management, or restoration) can be taken. Previous work has made important but limited contributions to understanding threats to conservation assets. For example, several studies have focused on threats to forested ecosystems^{4–6} – leaving a paucity of practical knowledge about threats to the remaining 70% of the Earth's terrestrial surface. Others have modeled future land use changes associated with specific drivers, primarily cropland and urban expansion^{7–9} – leaving research gaps regarding other important drivers of change. For example, energy, mining, and related infrastructure have been projected to cause 40% of land use change by 2050¹⁰. Additionally, studies often predict future land use change based on empirically-derived transitions from historical time series of remotely sensed imagery^{11,12}. Relying on these historical patterns of conversion can fail to capture future change^{11,13}, especially when not considering the geophysical and technological potential for future development. Without a consistent methodology to map future conversion pressures across all terrestrial habitats and across key drivers, we will likely miss many critical hotspots of threatened biodiversity and carbon stores where conservation interventions should be focused^{14–16}. This knowledge gap undermines our ability to achieve ambitious conservation goals efficiently and equitably, such as the commitments made by over 200 countries to conserve 30% of their lands and waters by 2030 (30×30) under the Kunming-Montreal Global Biodiversity Framework (K-M GBF) and the climate goals made by the 196 signatories to the United Nations Paris agreement.

¹Global Protect Oceans, Lands and Waters, The Nature Conservancy, Fort Collins, CO, 80524, USA. ²Global Science, The Nature Conservancy, Fort Collins, CO, 80521, USA. ³Global Science, The Nature Conservancy, Brunswick, ME, 04011, USA. ⁴Natural Climate Solutions Science, The Nature Conservancy, Arlington, VA, 22203, USA. ⁵CSIRO Environment, Brisbane, Queensland, 4102, Australia. ⁶Conservation Planning Technologies, Fort Collins, CO, 80521, USA. ⁷One Earth, Los Angeles, CA, 90039, USA. ✉e-mail: joakleaf@tnc.org

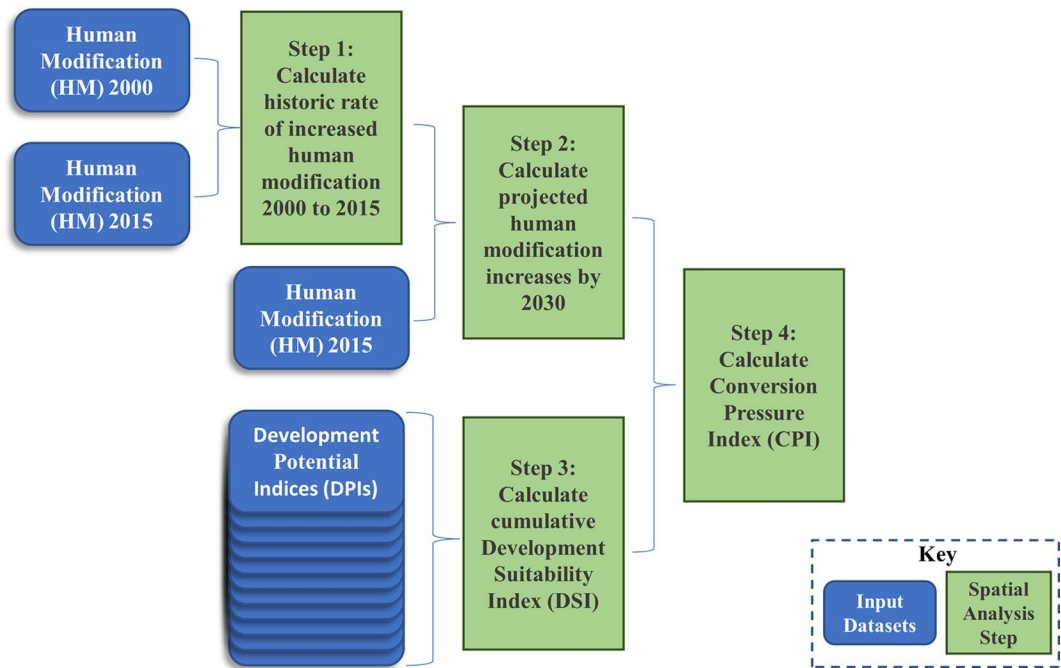


Fig. 1 Flow diagram of the input datasets and spatial analysis steps taken to create the conversion pressure index (CPI). Foundational to the development of the CPI are the 2000 and 2015 human modification (HM) maps and 14 development potential indices (DPIs). HM estimates cumulative impacts for a given year based on the spatial extent and intensity of impacts from human settlement, agriculture, forestry, transportation, mining, energy production, electrical infrastructure, dams, pollution, and human accessibility. DPIs are global maps that depict suitability for future renewable energy, oil and gas, mining, agriculture, and urban development.

Here, we developed the conversion pressure index (CPI): a global, spatially explicit, 1-km resolution map of future conversion pressure on land. The CPI estimates conversion pressure by combining spatially explicit data on historic rates of human modification with suitability for potential expansion by large-scale development from multiple sectors. We projected increases in human modification to 2030 based on historic patterns identified from a consistent, temporal sequence of human modification (HM¹). The HM estimates cumulative impacts from industrial pressures based on the spatial extent and intensity of impacts from human settlement, agriculture, forestry, transportation, mining, energy production, electrical infrastructure, dams, pollution, and human accessibility¹. To ensure the CPI accounts for a location's suitability for future conversion by agriculture, renewable energy, oil and gas, mining, and urbanization, we combined the projected HM map with published development potential indices (DPIs¹⁷) using an equal weighted fuzzy sum. This approach recognizes that land conversion is often correlated with previous development growth patterns^{18–22}, but that future expansion can deviate from historical trajectories and spatial patterns due to novel drivers^{11,13,23}.

We validated the CPI by producing a 2015 version that was then compared with observed human modification in the same year; and found strong agreement between the modeled and observed maps. This 2015 CPI version required applying our same methods but utilized maps of HM for 2000 and 2010 to test our methods. Additionally, we compared conversion pressure estimates from the CPI to a recently published future land use change model²⁴ and found notable differences. We attribute these differences to the cumulative mapping approach used for the CPI (versus a typical categorical approach) and discuss the benefits of capturing conversion pressure as a gradient of potential habitat loss.

The CPI provides a globally consistent, comprehensive, and spatially explicit tool to assess future conversion pressure from multiple sectors. It reveals that nearly 23% (3,038 million ha) of all lands have relatively high conversion pressure from industrial sectors. High conversion pressure is distributed across 200 countries and has the potential to impact over 460 million ha of intact natural lands critical for biodiversity, carbon storage, and ecosystem function^{25,26}. We illustrate how the CPI can be used to target regions (ecoregions, biomes, countries) where increased attention and proactive conservation can cost-effectively avert biodiversity and ecosystem loss and help meet global conservation targets.

Methods

Approach. The CPI is produced in four steps (Fig. 1). First, we estimated the historic rate of increased human modification from 2000 to 2015 using HM for years 2000 and 2015¹. Second, we projected where human modification was expected to increase by 2030, assuming a constant, annualized rate of change derived from the historic rate. We targeted the year 2030 given that it coincides with the targets of the K-M GBF and related national-level protection and conservation commitments¹⁴. Third, we produced a cumulative development suitability index (DSI) to emphasize areas susceptible to further development based on the presence of current

infrastructure and resources supporting rapid development potential. The DSI map was created as a composite of sector-specific development potential indices (DPIs) that captures a location's suitability for development by renewable energy, oil and gas, mining, agriculture, and expansion of urban sectors^{1,27}. All DPIS were relativized by country and were classified ordinally from 0 to 6 to establish seven relative categories of suitability for each pixel (i.e., none, very low, low, medium-low, medium-high, high, and very high). The DSI map was then created by using the mean and the maximum pixel values of all individual DPIS, both of which were shown to highlight areas of HM increases. For the final step, we produced the conversion pressure index (CPI) by combining a map of projected 2030 human modification increases with the cumulative DSI map to identify areas with high (1) to low (0) future land conversion pressure. By combining these two maps, we identify areas with high, historical rates of change, as well as areas with lower historical rates of change but high suitability for future industrial development.

Calculate historic rate of increased human modification. We calculated a historic rate of human modification using two HM maps spanning a 15-year period (HM_{2000} and HM_{2015})^{1,27}. The value of each pixel of the HM datasets ranges from 0 to 1, estimating the degree to which human activities in the post-industrial era have altered lands. A value of zero indicates negligible modification and a value of one indicates complete modification. HM accounts for human stressors that cause land conversion (i.e., human settlement, agriculture, forestry, transportation, mining, energy production, electrical infrastructure, and dams) and additional stressors that cause land degradation (i.e., pollution and human intrusion). We used HM_{2000} and HM_{2015} because these are the most recent and comparable datasets and provided an interval of 15 years that precedes and is of equivalent length to our 2015–2030 projection interval.

To calculate the rate of modification (ROM), we adapted the standardized rate of change formula proposed by Puyravaud²² (Eq. 1), which is derived from the continuously compound interest equation and commonly used to calculate annual rates of deforestation^{28,29}. We calculated ROM as follows:

$$ROM = \frac{\ln\left(\frac{(1 - HM_{2015})}{(1 - HM_{2000})}\right)}{-n} \quad (1)$$

where n is the number of years between the two time periods ($n = 15$ years) (see Supplementary Information, Text S1: Applying standardized rate of change formula to derive rate of modification and future HM). Note that this formula produces positive and negative rates, indicating areas where modification increased or decreased, respectively.

To account for the influence of neighboring areas, we made this calculation at multiple scales for each 300 m cell using circular neighborhoods of 1 km, 5 km, 10 km, and 25 km radii as informed by edge distance distributions of the degree of human modification of terrestrial habitat^{1,30}. Therefore, the average HM value for each neighborhood was applied iteratively to Eq. 1 and used to calculate a ROM for that radius. This produced four separate ROM maps that were subsequently weighted using an exponential distance decay formula (Eq. 2), which assumes that nearby disturbances have greater impact than those that are farther away. Following the approach of the Natural Capital Project³¹, we calculated:

$$i = e^{\frac{-2.99}{d_{max}} * d_i} \quad (2)$$

where d_{max} is our maximum neighborhood radius (i.e., 25 km) and d_i is assigned to each of the neighborhood radii (i.e., 1, 5, 10, 25 km). The resulting calculation produced weights for the four neighborhoods (i.e., 0.887, 0.550, 0.302, 0.050), which were subsequently scaled to sum to one (i.e., 0.496, 0.307, 0.169, 0.028). These scaled values were applied to a weighted sum of the four ROM maps to produce our multi-scaled ROM. We excluded values ≤ 0 , which represents 17% of all cells, to focus only on areas that experienced increasing human modification from 2000–2015 (Fig. 2).

Projected increase in human modification by 2030. To project increases in human modification by 2030 (HM_{2030}), we applied the $ROM_{i2015:2000}$ map to the HM_{2015} per Eq. 3 (see Supplementary Materials, Text S1: Applying exponential decay formula to derive rate of modification and future HM):

$$HM_{2030} = 1 - (1 - HM_{2015}) * e^{-15 * ROM_{i2015:2000}} \quad (3)$$

We then subtracted HM_{2030} from HM_{2015} to estimate the amount of increase in modification by 2030 ($HM_{Increase_{2030}}$; Figure S1).

To better distribute and differentiate relative values of human modification increases, we applied a maximum threshold to $HM_{Increase_{2030}}$ map identified by the 99.999th percentile HM increase value (0.2585). We then assigned all pixels with HM values above this threshold ($= > 0.2585$ to 0.519) a value of 0.2585 to eliminate extreme outliers. Finally, to better differentiate across values, we transformed all values by calculating the cube root before finally scaling these transform values from 0 to 1 to generate the $HM_{Increase_{2030scaled}}$ map (Fig. 3). We applied a cube root transformation due to extreme right skewness of the HM increases and selected this transformation method to improve the interpretability of data and mapped patterns. For example, a $HM_{Increase_{2030scaled}}$ value of 0.5 estimates a HM increase of 0.032, a jump which may cause over 3% of the global low HM to become classified as moderate, while values over 0.75 equate to HM increases of 0.1 or greater which could potentially shift completely unmodified lands to moderate modification. The $HM_{Increase_{2030scaled}}$ map had a global median value of approximately 0.178 with Q1 and Q3 values of 0 and 0.428, respectively.

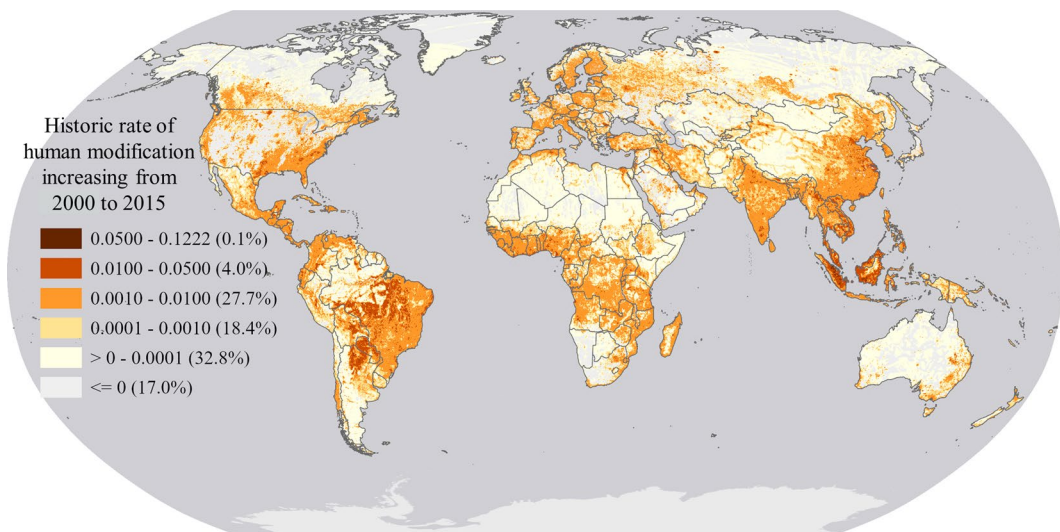


Fig. 2 Global map of historic rate of human modification increasing from 2000 to 2015 ($ROM_{i2015,2000}$). Areas of increased modification are emphasized, with the highest rates in dark red and the lowest rates in yellow. Land areas in gray had no increase in modification during the 15-year time span. Classes are user-defined, with the percentage of land (excluding Antarctica) shown in parentheses.

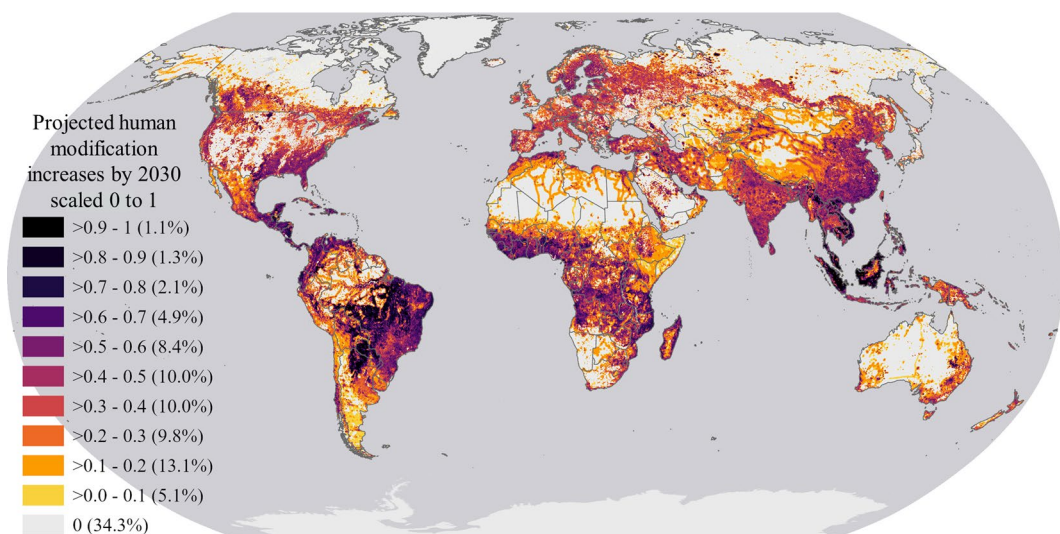


Fig. 3 Global map of projected increase in human modification from 2015 to 2030 scaled 0 to 1 ($HM_{Increase2030scaled}$). The highest projected increase is shown in black, the lowest projected increase in gold, and land areas in gray have no projected increase in modification. Classes are equal interval, with the percentage of land (excluding Antarctica) shown in parentheses.

Cumulative development suitability index. To capture potential conversion associated with new and emerging pressures, we created a cumulative development suitability index (DSI) derived from previously published, sector-specific development potential indices (DPIs)^{17,32} and an additionally derived DPI for urban expansion³³. DPIs are global, spatially explicit, 1-km resolution and aligned maps that depict suitability for renewable energy (concentrated and photovoltaic solar power, wind power, and hydropower), oil and gas (conventional and unconventional), mining (coal, metallic and non-metallic mining), and agriculture (crop and biofuels expansion) development. Each DPI has a standardized 0 – 1 value that indicates its suitability based on: (a) sector-specific land constraints on development (e.g., suitable land cover, slope); (b) land suitability for sector expansion based on resource availability (sector-specific yields); and (c) siting feasibility of new development (e.g., ability to transport resources or materials, access to demand centers, and proximity of existing development).

Each DPI was binned into six suitability categories, following Oakleaf *et al.*¹⁷ recommended z-score binning: very low (≤ -1.282), low ($> -1.282 - 0.675$), medium-low ($> -0.675 - 0.000$), medium-high ($> 0.000 - 0.675$), high ($> 0.675 - 1.282$), and very high (> 1.282). We used z-scores, mean-standardized by country, based on the assumption that regional resource extraction dynamics can shift in unison at the scale of a national market.

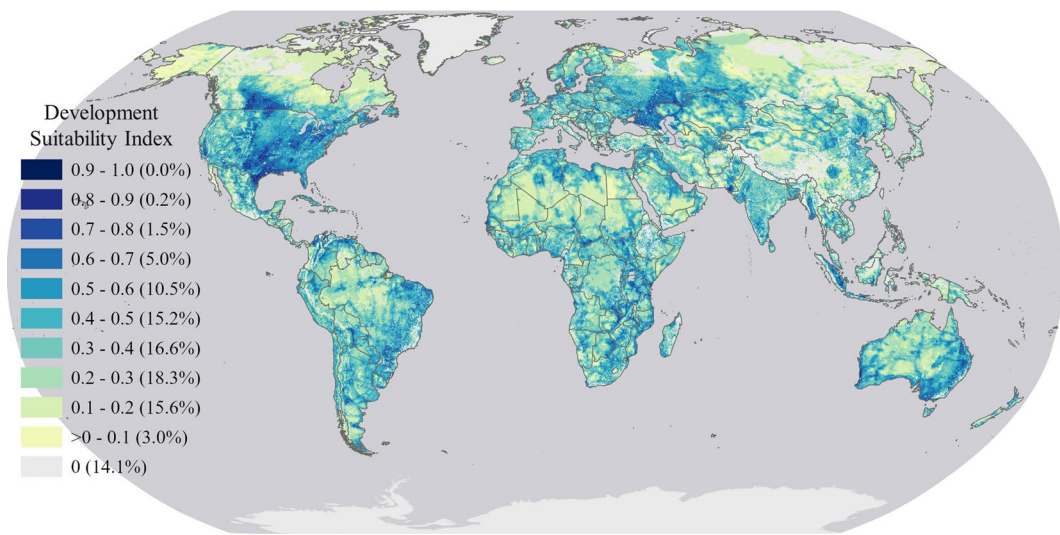


Fig. 4 Global map of development suitability index (DSI) on land. The DSI map ranks development suitability scores from 0 (lowest) to 1 (highest) based on the average score across all development potential indices (DPIS) multiplied by the maximum score. These scores were square root transformed and scaled from 0 to 1 to produce the DSI map. Land areas in gray with a DSI of 0 were unsuitable for development across all 14 DPIS. Classes are equal interval, with the percentage of land (excluding Antarctica) shown in parentheses.

Relativizing DPI values within each country reduces bias toward economically developed countries, implicitly controls for economic growth that may vary across regions and recognizes that countries with relative suitability values lower than the global average will still undergo some level of development where access to and demand for resources exists. Lastly, because the urban DPI was derived from urban expansion probabilities based on population growth projections³³ that were more restrictive than the methods applied to the other sector-specific DPIS which only identified suitability measures (e.g., suitable areas for urban expansion following DPI methodology may be ranked based on proximity to roads, existing urban areas and slope but would not be limited by projected population growth), we binned the lower and upper 50th percentiles of non-zero urban DPI values into high or very high suitability categories, respectively.

We then applied a simple, ordinal rank to the categories of all 14 DPIS (i.e., 0 = unsuitable, 1 = very low, 2 = low, 3 = medium low, 4 = medium high, 5 = high, and 6 = very high), and subsequently combined these 14 DPIS into one cumulative global development pressure map (Figure S2) by selecting the maximum value per pixel across all DPIS (e.g.^{34–36}). Additionally, we calculated the mean values of all 14 ranked DPIS which produced a map with values ranging from 0 to 4.57 (Figure S3). Since both approaches (i.e., maximum and mean) proved to capture past human modification gains as values increased and with the mean values showing a positive correlation with human modification gains per pixel (see Supplementary Information, Text S2: Extended Validation), we applied a hybrid approach to creating the DSI by multiplying the mean value across all 14 DPIS by the maximum value. We observed that when compared to the simple mean, multiplying the mean value by the maximum value improved the ability to estimate how suitable a pixel is for development (see Supplementary Materials, Text S2: Extended Validation). To illustrate the added value of this hybrid approach, a pixel overlapping with two medium low categories produces a DS score of 1.29 (i.e., 6/14*3) whereas a pixel overlapping one very high category produces a DS score of 2.57 (i.e., 6/14*6). Had we relied only on the simple mean, an equivalent value of 0.43 (i.e., 6/14) would have been generated for both pixels despite important contextual differences. This method created global DSI scores ranging from 0 to 27.429 (Figure S4) and continued capturing past changes while being positively correlated to human modification gains per pixel (see Supplementary Information, Text S2: Extended Validation). Lastly, to better spread the distribution of DSI scores, we applied a square root transformation and scaled values from 0-1 to create a final development suitability index (DSI) map (Fig. 4). Again, we applied a transformation due to the right-skewness of these data however unlike the cube root transformation used to produce the *HM_Increase_{2030scaled}* map (Fig. 3), we used a square root transformation. This produced a global median of 0.288 and a Q1 and Q3 of 0.153 and 0.444, respectively (Fig. 4). Had we applied a cubed-root transformation, the global median would have been 0.437 with a Q1 and Q3 of 0.286 and 0.583, respectively. This distribution of values would have invertedly given the DSI more weight in producing the final CPI than the *HM_Increase_{2030scaled}* map. While the squared-root transformation still produced a slightly higher median for the DSI (i.e., 0.178 higher) the Q3 values were very similar with DSI only 0.016 higher and thus provide a distribution of values which could be used within the final formula used to produce the CPI.

Conversion pressure index. To produce a conversion pressure index (CPI), we combined the *HM_Increase_{2030scaled}* map with the DSI map using a fuzzy sum operator (Eq. 5):

$$\text{Conversion pressure index (CPI)} = 1 - ((1 - \text{HM}_\text{Increase}_{2030\text{scaled}}) \times (1 - \text{DSI})) \quad (5)$$

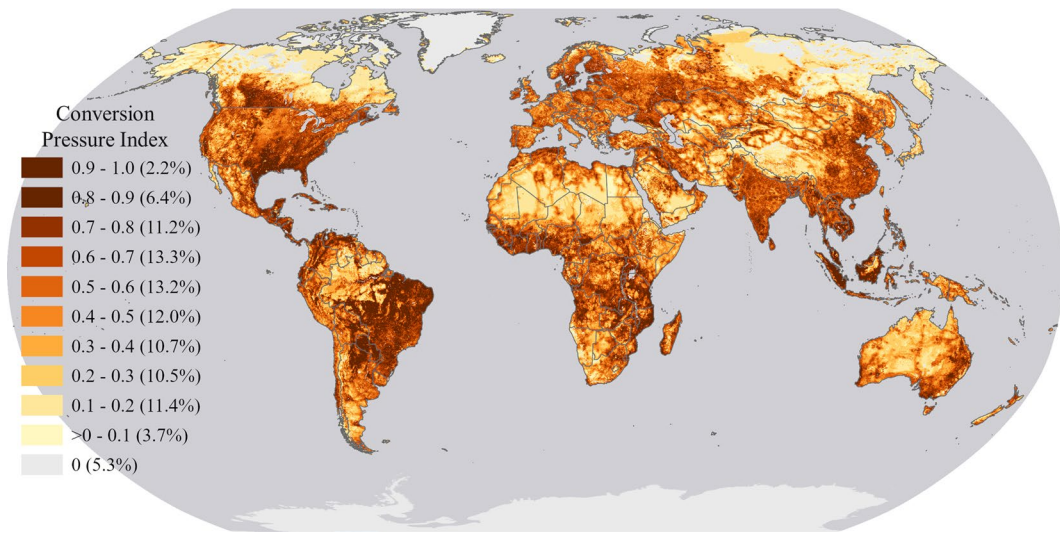


Fig. 5 Global map of the conversion pressure index (CPI), which scales conversion pressure from 0 (none) to 1 (high) based on projected increases in human modification derived from historic patterns combined with suitability for industrial development expansion. CPI is classified in equal intervals with the percentage of lands (excluding Antarctica) shown in parentheses.

We used the fuzzy sum operator to estimate overall conversion pressure because it accounts for the potential correlation among our two maps, limits cumulative values to never exceed 1, and improves upon a simple additive model by reducing the effects of double counting when values are high^{1,30,37}. CPI values therefore ranged from 0 to 1 and were driven by the contribution of both future human modification increases and high development suitability.

Finally, to reconcile with the coarsest resolution of our input data and to avoid assumptions of precision, we resampled the 300-m resolution CPI to 1-km resolution. To resample, we first created a 900-m resolution raster dataset by calculating the arithmetic mean for the nine, 300-m pixels found within each larger pixel and then applied bilinear interpolation to produce the final 1-km resolution dataset (Fig. 5), resulting in a global, 1-km resolution CPI with values ranging from 0 (no conversion pressure) to 1 (highest conversion pressure).

Data Records

Two CPI products are accessible via figshare³⁸ as GeoTIFF raster datasets: 1) the continuous 0–1 map and 2) a categorized version of the map. We mapped the CPI into six categories of conversion pressure, from very low to very high, using the global median value of the CPI for all lands (median = 0.471) and the median absolute deviation ($MAD = \pm 0.206$) for classification breakpoints. We used a median/median absolute deviation (mad) classification scheme rather than the common mean/standard deviation classification because the CPI data did not meet the assumption of normality due to instead having a slight right skewness. Thus, by using the median value, we relied on a central tendency value that is less affected by a skewed distribution³⁹. For example, all pixels with CPI values greater than 0.883 (median + 2*MAD) were classified as very high (Fig. 6). The Mollweide coordinate system was applied to both of these 1-km resolution, raster datasets. The CPI and all corresponding input data (see Fig. 1) can be viewed and examined interactively at <https://tnc-ps-web.s3.amazonaws.com/GDRA/CPI/index.html>.

Also accessible via figshare³⁸ we provide an Excel spreadsheet that calculates all critical CPI statistics: mean, standard deviation, median, amount of land classified as high or very high CPI, proportion of land classified as high or very high CPI, and the CPI category based on the global median/MAD breakpoints used in Fig. 6 by region, country, biome, and ecoregion. We find that nearly 23% of lands (3,036 million ha) have relatively high conversion pressure ($CPI > 0.677$, > 1 MAD above the global median). Hotspots of high conversion pressure occur in 200 different countries and span all continents excluding Antarctica, with 47 countries classified as having high conversion pressure (country median CPI > 0.677) and one country (Malaysia) classified as having very high conversion pressure (country median CPI > 0.884 , > 2 MAD above the global median). Of these 48 countries, 19 are in Africa, 13 in Central America, and the remaining 16 are in East and Southeast Asia³⁸.

In addition to countries, we evaluate conversion pressure within each biome and ecoregion based on the Dinerstein *et al.*⁴⁰ dataset which has been widely used for conservation prioritization^{7,9,41}. We find that 12 out of 14 terrestrial biomes have ecoregions with relatively high conversion pressure (ecoregion median CPI > 0.677). The tropical and subtropical dry broadleaf forests biome has nearly half of its ecoregions classified in the top two categories of conversion pressure³⁸. This biome is closely followed by mangroves, tropical and subtropical moist broadleaf forests, and flooded grasslands and savannas that have nearly one third of their ecoregions classified as having high conversion pressure.

Technical Validation

To validate the CPI, we followed our methods (Fig. 1) to produce a CPI for 2015 (CPI_{2015}) that we then compared with the actual HM increases identified from subtracting HM_{2010} from HM_{2015} ($HM_{\text{MappedGain}}_{2010:2015}$). We created the CPI_{2015} by first calculating the historic rate of human modification increasing from 2000 to 2010

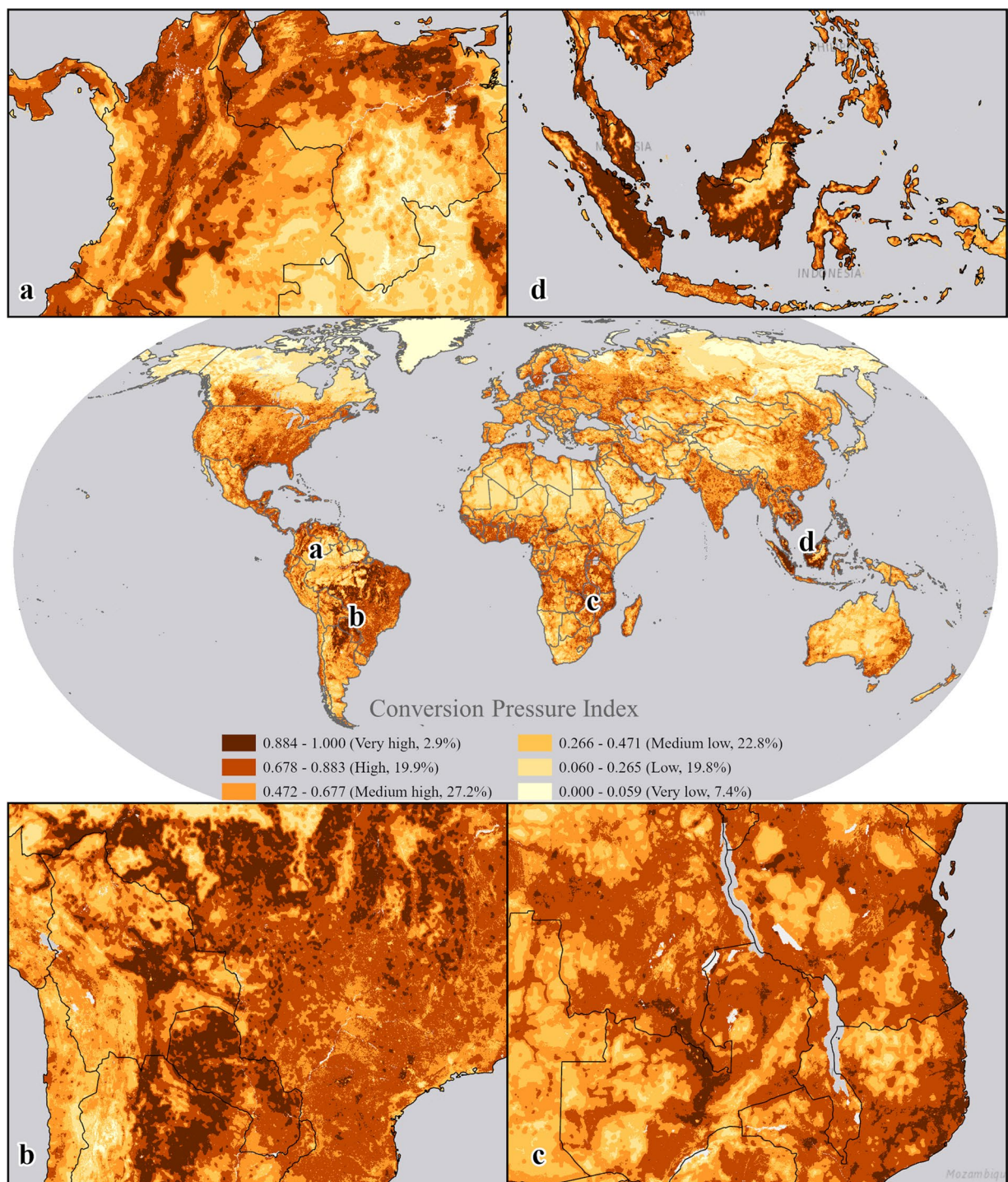


Fig. 6 Global map of the conversion pressure index (CPI), mapped into 6 categories based on the global median value of CPI for land (0.471) and the median absolute deviation (± 0.206). Very high and high CPI are shown in dark-brown and dark-red with breakpoints of $+2 \text{ MAD}$ and $+1 \text{ MAD}$ from the median, respectively. Four inset maps are provided, detailing regions with all classifications from very high to very low: (a) Colombia and Venezuela; (b) Argentina, Brazil, Bolivia, and Paraguay; (c) Democratic Republic of Congo, Mozambique, Tanzania, and Zambia; and (d) Indonesia, Malaysia, and Philippines.

($ROM_{i2010:2000}$) to model HM increases in 2015 from 2010. We then scaled these modeled HM increases from 0-1 following the same techniques ($HM_Increase_{2015scaled}$) and combined them with the DSI map using a fuzzy sum operator (see Eq. 5). We selected this time frame to model the CPI (2000 to 2010) and subsequent HM increase (2010 to 2015) due to it being the most recent mapped HM change data available while also being within the time frame used in producing the CPI. For detailed descriptions of how CPI_{2015} was created and further validation of all data inputs into this version of the CPI, see Supplementary Information, Text S2: Extended validation.

On average, the highest HM_MappedGain_{2010:2015} values occurred in the highest CPI₂₀₁₅ range ($>0.90\text{--}1.00$) with a mean gain of 0.102 ($\pm 1\text{ SD} = 0.067$) and 50% of the gains being greater than 0.092 (Table S1). Encouragingly, both the mean and median gain for each bin lessened as the CPI bin values decreased. When examining the distribution of HM gains within each CPI bin across a range of percentile values (i.e., 5, 25, 50, 75, and 95), this pattern continued. The top three ranges of scores (CPI > 0.70) covered approximately 14% of the globe but contained over 55% of the total modification increases. This same range of values contained over 70% of the top 10% of mapped change occurring from 2010 to 2015, and yet only contained 4% of the pixels without any increase. Within these 4%, most pixels were found in moderately modified lands (mean 2015 HM = 0.29, $\pm 1\text{ SD} = 0.22$) and were identified as having moderately high DSI (DSI mean = 0.61, $\pm 1\text{ SD} = 0.11$). While these lands did not incur modification changes during the 5 years examined, there is a strong potential for future industrialized development by several sectors that often replace agricultural lands (e.g., urban, PV solar, oil and gas).

Overall, these validation results indicated the CPI₂₀₁₅ was performing as anticipated by capturing large modification changes in the high values and providing a relative ranking of change as it decreased to zero. Although both input maps (i.e., HM_Increase_{2015scaled} and DSI) also showed positive results in capturing modification gains, when combined to produce the CPI₂₀₁₅, a stronger ranking of where these gains occurred was produced.

Usage Notes

Integrating the CPI into conservation prioritization. Mapping the distribution and gradient of land conversion pressure from multiple development sectors is critical to identifying regions (e.g., ecoregions, biomes, or countries) where increased attention is warranted to avert the risk of ecosystem or biodiversity loss. It can also help identify where to focus allocation of funding and resources for conservation interventions and policy measures. For example, the CPI can be used to map “Anthropocene refugia”⁴² prioritize areas of global importance for biodiversity³⁵ and nature’s contributions to people³⁶, and identify places where actions and interventions might be needed to strengthen Indigenous stewardship and governance³⁴.

Regardless of the asset being considered (e.g., natural habitat, intact lands, carbon stores, forests, ecosystem services, biodiversity, endemic or endangered species, livelihoods, food security, significant cultural resources), it is important that the CPI be used across an application-relevant unit of comparison (e.g., biome, ecoregion, country, and/or state) and that the conversion pressures of these units be assessed and described relative to this set (for more detail on this process, see Supplementary Information, Text S3: Detailed example of applying the CPI to a global conservation prioritization at an ecoregional level). We provide a global CPI with values that range from 0 –1, allowing users to aggregate the CPI and determine appropriate categories and break points for the scale of their analysis. While we offer one approach to classifying ecoregional CPI values relative to the global median and MAD, we acknowledge that there are many ways of creating such classifications. For example, others have used percentiles such as the top 10% or top 20% as priority hotspots³⁵.

Comparing CPI to future land use change models. Some global, conservation prioritization efforts have relied on projected categorical land use transitions using exploratory scenarios and alternative futures, such as those associated with shared socioeconomic pathways (SSPs)^{43,44}. This approach has been used to estimate global habitat loss^{7,9} and wilderness loss⁸. Such assessments have used different landcover datasets and future scenarios, varying temporal and spatial resolutions, and different proxies for conservation assets, thereby identifying different global conservation priorities. For example, Gonçalves-Souza *et al.*⁹ examined conversion across all lands, whereas Allan *et al.*⁷ and Cao *et al.*⁸ limited their analysis to only areas with low human impact. Allan *et al.*⁷ focused on “natural lands” at risk of future conversion based on a Human Footprint⁴⁵ score of <5 in areas outside of protected areas, key biodiversity areas, and wilderness areas. While these studies advance our understanding of habitat conversion threats, they are restricted in the range of drivers and geographies considered, and do not consider a gradient of conversion pressure that may deviate from historic patterns. For example, undiscovered or undeveloped resources (e.g., mineral and/or oil and gas deposits) or new technologies (e.g., oil and gas fracking, solar and/or wind) can lead to unprecedented, rapid development of lands that may be spatially disconnected to well observed conversion frontiers²³. In addition, land use change models often focus on agriculture and urban expansion^{11,15}. While these sectors have driven habitat loss, they often coincide with one another (e.g., urban replacing cropland^{46,47}) and should be considered in conjunction with other sectors to capture cumulative ecosystem pressures¹⁰. The CPI is meant to fill this information gap and when compared to land use change models often expands and/or deviates from predicted future land use changes (for more details see Supplementary Information: Text S4: Comparing CPI to habitat loss estimates from a land cover change model).

Data caveats. We produced the CPI specifically to provide a relative global and/or regional comparison of conversion pressure. The CPI does not indicate the amount of conversion to be expected, nor does it highlight areas transitioning from variable definitions of “natural” to converted. The CPI does offer a means of comparing threat to lands of critical importance to biodiversity or ecosystem services using a much broader set of drivers than those captured by land cover change mapping (e.g., forest to cropland) and provides an ability to assess pressures beyond the conversion frontier. Additionally, the CPI covers all lands, which allows for consideration of lands outside of what is typically targeted, including partially converted or degraded lands which may be important for supporting biodiversity and ecosystem services⁴⁸.

We relied on two open-access databases for the creation of the CPI: the 2000 and 2015 temporal HM¹, and the 14 DPIs¹⁷. Updates and improvements to either of these datasets will undoubtedly influence the CPI. For example, a 2020 version of the temporal HM would provide greater resolution and insight on where future conversion may happen. Additionally, our approach for modeling future 2030 HM increases was intentionally conservative but could be adapted to better capture areas on the “tipping point” of substantial HM increases.

With regards to DSI, an intermediate product in the creation of the CPI, we relied on the 14 DPIS due to a lack of other comparable and consistent data being publicly available. While the DSI map correlated with HM increases, future work could be centered on the use of variables with more direct influence on human modification change. Finally, the global CPI does not capture potentially important contextual information that is often available only at more local scales (e.g., leases, environmental regulations, incentives, tax breaks, varying market changes, technological advancements and/or planned infrastructure development) all of which influence future development siting and should be considered in more local scale applications.

Code availability

No code was produced to support this effort. All analyses described in this paper utilized current available tools within ESRI mapping software ArcGIS Pro 3x and required use of the Spatial Analyst extension of this software (esri.com). All analyses can also be accomplished within QGIS (qgis.org), an open-source mapping software.

Received: 26 March 2024; Accepted: 11 July 2024;

Published online: 30 July 2024

References

- Theobald, D. M. *et al.* Earth transformed: Detailed mapping of global human modification from 1990 to 2017. *Earth System Science Data* **12**, 1953–1972 (2020).
- Cardinale, B. J. *et al.* Biodiversity loss and its impact on humanity. *Nature* **486**, 59–67 (2012).
- Jaureguiberry, P. *et al.* The direct drivers of recent global anthropogenic biodiversity loss. *Science Advances* **8**, eabm9982 (2022).
- Curtis, P. G., Slay, C. M., Harris, N. L., Tyukavina, A. & Hansen, M. C. Classifying drivers of global forest loss. *Science* **361**, 1108–1111 (2018).
- d'Annunzio, R., Sandker, M., Finegold, Y. & Min, Z. Projecting global forest area towards 2030. *Forest Ecology and Management* **352**, 124–133 (2015).
- Hewson, J., Crema, S. C., González-Roglich, M., Tabor, K. & Harvey, C. A. New 1 km Resolution Datasets of Global and Regional Risks of Tree Cover Loss. *Land* **8**, 14 (2019). *2019, Vol. 8, Page 14*.
- Allan, J. R. *et al.* The minimum land area requiring conservation attention to safeguard biodiversity. *Science* **376**, 1094–1101 (2022).
- Cao, Y. *et al.* Potential wilderness loss could undermine the post-2020 global biodiversity framework. *Biological Conservation* **275**, 109753 (2022).
- Gonçalves-Souza, D., Verburg, P. H. & Dobrovolski, R. Habitat loss, extinction predictability and conservation efforts in the terrestrial ecoregions. *Biological Conservation* **246**, 108579 (2020).
- Johnson, J. A. *et al.* Energy matters: Mitigating the impacts of future land expansion will require managing energy and extractive footprints. *Ecological Economics* **187**, 107106 (2021).
- Verburg, P. H. *et al.* Beyond land cover change: towards a new generation of land use models. *Current Opinion in Environmental Sustainability* **38**, 77–85 (2019).
- Long, H., Zhang, Y., Ma, L. & Tu, S. Land Use Transitions: Progress, Challenges and Prospects. *Land* **10**, 903 (2021).
- Dalla-Nora, E. L., de Aguiar, A. P. D., Lapola, D. M. & Woltjer, G. Why have land use change models for the Amazon failed to capture the amount of deforestation over the last decade? *Land Use Policy* **39**, 403–411 (2014).
- Nicholson, E. *et al.* Scientific foundations for an ecosystem goal, milestones and indicators for the post-2020 global biodiversity framework. *Nature Ecology & Evolution* **5**, 1338–1349 (2021).
- Watson, J. E. M., Ellis, E. C., Pillay, R., Williams, B. A. & Venter, O. Mapping Industrial Influences on Earth's Ecology. *Annual Review of Environment and Resources* **48**, 289–317 (2023).
- Virtanen, E. A., Söderholm, M. & Moilanen, A. How threats inform conservation planning—A systematic review protocol. *PLOS ONE* **17**, e0269107 (2022).
- Oakleaf, J. *et al.* Mapping global development potential for renewable energy, fossil fuels, mining and agriculture sectors. *Scientific Data* **6**, 101 (2019).
- Geist, H. *et al.* Causes and Trajectories of Land-Use/Cover Change. *Land-Use and Land-Cover Change* 41–70, https://doi.org/10.1007/3-540-32202-7_3 (2006).
- Harris, N. L. *et al.* Using spatial statistics to identify emerging hot spots of forest loss. *Environmental Research Letters* **12**, 024012 (2017).
- Linkie, M., Smith, R. J. & Leader-Williams, N. Mapping and predicting deforestation patterns in the lowlands of Sumatra. *Biodiversity and Conservation* **13**, 1809–1818 (2004).
- Meyer, W. B. & Turner, B. L. Human Population Growth and Global Land-Use/Cover Change. *Annual Review of Ecology and Systematics* **23**, 39–61 (1992).
- Puyravaud, J. P. Standardizing the calculation of the annual rate of deforestation. *Forest Ecology and Management* **177**, 593–596 (2003).
- Meyfroidt, P. *et al.* Ten facts about land systems for sustainability. *Proceedings of the National Academy of Sciences* **119**, e2109217118 (2022).
- Chen, M. *et al.* Global land use for 2015–2100 at 0.05° resolution under diverse socioeconomic and climate scenarios. *Scientific Data* **7**, 1–11 (2020).
- Watson, J. E. M. *et al.* The exceptional value of intact forest ecosystems. *Nat Ecol Evol* **2**, 599–610 (2018).
- Riggio, J. *et al.* Global human influence maps reveal clear opportunities in conserving Earth's remaining intact terrestrial ecosystems. *Global Change Biology* **26**, 4344–4356 (2020).
- Theobald, D. M. *et al.* Data for detailed temporal mapping of global human modification from 1990 to 2017. *Zenodo* <https://doi.org/10.5281/zenodo.3963013> (2020).
- Munteanu, C. *et al.* Forest and agricultural land change in the Carpathian region—A meta-analysis of long-term patterns and drivers of change. *Land Use Policy* **38**, 685–697 (2014).
- Panday, P. K. *et al.* Deforestation offsets water balance changes due to climate variability in the Xingu River in eastern Amazonia. *Journal of Hydrology* **523**, 822–829 (2015).
- Kennedy, C. M., Oakleaf, J. R., Theobald, D. M., Baruch-Mordo, S. & Kiesecker, J. Managing the middle: A shift in conservation priorities based on the global human modification gradient. *Global Change Biology* **25**, 811–826 (2019).
- Natural Capital Project. *InVEST 3.14.1 User's Guide*. <https://naturalcapitalproject.stanford.edu/software/invest> (2024).
- Oakleaf, J. R. *et al.* Global development potential indices for renewable energy, fossil fuels, mining and agriculture sectors. *figshare* <https://figshare.com/s/f846f9331bd10e5efd9> (2019).
- Zhou, Y., Varquez, A. C. G. & Kanda, M. High-resolution global urban growth projection based on multiple applications of the SLEUTH urban growth model. *Scientific Data* **6**, 34 (2019).

34. Kennedy, C. M. *et al.* Indigenous Peoples' lands are threatened by industrial development; conversion risk assessment reveals need to support Indigenous stewardship. *One Earth* **6**, 1032–1049 (2023).
35. Wolff, N. H. *et al.* Prioritizing global land protection for population persistence can double the efficiency of habitat protection for reducing mammal extinction risk. *One Earth* **6**, 1564–1575 (2023).
36. Neugarten, R. A. *et al.* Mapping the planet's critical areas for biodiversity and nature's contributions to people. *Nat Commun* **15**, 261 (2024).
37. Malczewski Jacek. *GIS and Multicriteria Decision Analysis*. (Wiley, 1999).
38. Oakleaf, J. *et al.* Conversion Pressure Index. *figshare* <https://doi.org/10.6084/m9.figshare.25340668> (2024).
39. Kaur, P., Stoltzfus, J. & Yellapu, V. Descriptive statistics. *International Journal of Academic Medicine* **4**, 60 (2018).
40. Dinerstein, E. *et al.* An Ecoregion-Based Approach to Protecting Half the Terrestrial Realm. *BioScience* **67**, 534–545 (2017).
41. Dinerstein, E. *et al.* A Global Deal For Nature: Guiding principles, milestones, and targets. *Science Advances* **5**, eaaw2869 (2019).
42. Monserrat, S., Jarvie, S. & Svenning, J.-C. Anthropocene refugia: integrating history and predictive modelling to assess the space available for biodiversity in a human-dominated world. *Philosophical Transactions of the Royal Society B: Biological Sciences* **374**, 20190219 (2019).
43. Riahi, K. *et al.* The Shared Socioeconomic Pathways and their energy, land use, and greenhouse gas emissions implications: An overview. *Global Environmental Change* **42**, 153–168 (2017).
44. van Vuuren, D. P. *et al.* The representative concentration pathways: An overview. *Climatic Change* **109**, 5–31 (2011).
45. Venter, O. Changes in the global Human Footprint and implications for biodiversity conservation. *Proceedings of the National Academy of Sciences of the United States of America*.
46. Bren d'Amour, C. *et al.* Future urban land expansion and implications for global croplands. *Proceedings of the National Academy of Sciences* **114**, 8939–8944 (2017).
47. Huang, Q. *et al.* The occupation of cropland by global urban expansion from 1992 to 2016 and its implications. *Environ. Res. Lett.* **15**, 084037 (2020).
48. Grass, I., Batáry, P. & Tscharntke, T. Chapter Six - Combining land-sparing and land-sharing in European landscapes. in *Advances in Ecological Research* (eds. Bohan, D. A. & Vanbergen, A. J.) vol. 64 251–303 (Academic Press, 2021).

Acknowledgements

The Nature Conservancy – Global Protect 30 × 30 Strategy, Bezos Earth Fund and One Earth for funding project. Glenn Moncrieff for reviewing materials. Dr. Emmet Brown for providing insight and guidance regarding past and future human modification changes.

Author contributions

J.O., C.K., N.W., D.E.T.H., K.B. and J.K. conceived and designed the study; J.O. applied all methods and produced all data; J.O. conducted validation and usage analyses; J.O., C.K., N.W., D.E.T.H., P.E., D.T., B.F., K.B. and J.K. reviewed all analyses; J.O. and B.F. produced figures and tables; J.O., C.K., B.F. and J.K. interpreted usage; J.O., C.K., B.F. and J.K. designed and wrote the paper; J.O., C.K., B.F., N.W., D.E.T.H., P.E., D.T., K.B. and J.K. revised the paper.

Competing interests

The authors declare no competing interests.

Additional information

Supplementary information The online version contains supplementary material available at <https://doi.org/10.1038/s41597-024-03639-9>.

Correspondence and requests for materials should be addressed to J.O.

Reprints and permissions information is available at www.nature.com/reprints.

Publisher's note Springer Nature remains neutral with regard to jurisdictional claims in published maps and institutional affiliations.



Open Access This article is licensed under a Creative Commons Attribution-NonCommercial-NoDerivatives 4.0 International License, which permits any non-commercial use, sharing, distribution and reproduction in any medium or format, as long as you give appropriate credit to the original author(s) and the source, provide a link to the Creative Commons licence, and indicate if you modified the licensed material. You do not have permission under this licence to share adapted material derived from this article or parts of it. The images or other third party material in this article are included in the article's Creative Commons licence, unless indicated otherwise in a credit line to the material. If material is not included in the article's Creative Commons licence and your intended use is not permitted by statutory regulation or exceeds the permitted use, you will need to obtain permission directly from the copyright holder. To view a copy of this licence, visit <http://creativecommons.org/licenses/by-nc-nd/4.0/>.

© The Author(s) 2024